Indoor Radio Map Construction and Localization With Deep Gaussian Processes

Xiangyu Wang, Xuyu Wang, *Member, IEEE*, Shiwen Mao, *Fellow, IEEE*, Jian Zhang, *Member, IEEE*, Senthilkumar C. G. Periaswamy, and Justin Patton

***Abstract*—With the increasing demand for location-based service, WiFi-based localization has become one of the most popular methods due to the wide deployment of WiFi and its low cost. To improve this technology, we propose DeepMap, a *deep* Gaussian process for indoor radio *map* construction and location estimation. Received signal strength (RSS) samples are used in DeepMap to generate accurate and fine-grained radio maps. A two-layer deep Gaussian process model is designed to determine the relationship between the location and RSS samples, while the model parameters are optimized with an offline Bayesian training method. To identify the location of a mobile device, a Bayesian fusion method is proposed, which leverages RSS samples from multiple access points (APs) to achieve high location estimation accuracy. We conduct comprehensive experiments to verify the performance of DeepMap in two indoor settings. DeepMap's robustness is validated using limited training data.**

***Index Terms*—Deep Gaussian process, deep learning, indoor localization, radio map construction.**

I. Introduction

LOCATION-BASED service has drawn great interest in the industry and research community [1]–[5], largely due to the popularity of mobile devices and wide deployment of wireless networks. However, producing accurate location estimates for mobile devices using radio-frequency (RF) signals is still a challenging problem. This is because RF signals propagate unpredictably in indoor environments (e.g., the multipath effect degrades the localization precision of many indoor localization systems [6]–[10]). To address the problem of accuracy degradation that results from the complex signal propagation indoors, fingerprinting-based localization approaches have gained notoriety and shown high promise. A fingerprinting-based localization approach consists of an offline stage and an online stage. Fingerprints, in the form of RF signal features and location pair, are collected and stored in the offline stage, consisting of exhaustive records of the serviced area. In the online stage, location estimation is obtained by comparing the newly collected records to the stored fingerprints [11].

Owing to its low hardware requirement and ubiquitous use, the received signal strength (RSS) of WiFi signals has been leveraged as fingerprints in many proposed localization systems. In the seminal work [12], the RSS was utilized as fingerprints for the first time. Moreover, Youssef and Agrawala [13] developed a discrete-space estimator for high localization accuracy of an RSS-based fingerprinting system. In more recent years, the channel state information (CSI) has gained much attention from researchers because it carries fine-grained information of the wireless channel estimated from each subcarrier [14]–[19]. However, the density of fingerprints is a key factor that significantly affects the accuracy of indoor fingerprinting. To achieve high-accuracy localization, a wardrive is essential for fingerprint collection, which is usually time consuming and laborious.

To reduce the dependency on wardriving, a radio map can be constructed with discrete training data in some localization systems. The Gaussian process is a useful method for building such radio maps. Regarding cellular networks, a Gaussian process was used in the GPPS system for generating radio maps [20]. In GPPS, the distribution of signal strength was modeled by a Gaussian process and an unknown location was estimated by maximizing a joint likelihood of RSSs with respect to the position. Furthermore, a Gaussian process regression (GPR) was utilized to model the relationship of signal strength and location in many positioning systems [21]–[26]. With a model regressed by a Gaussian process, the distance between mobile devices and access points (APs) could be conveniently inferred, and the estimated location of the mobile device can be obtained by triangulation. However, to locate mobile devices, it is necessary to know the accurate locations of the APs. In many real-world scenarios, it is usually hard, if not impossible, to acquire the precise coordinates of the surrounding APs.

A Gaussian process is depicted by its mean and covariance functions. According to [20]–[26], Gaussian processes are capable of measuring the uncertainty in the RSS data over a continuous space. It belongs to the class of Bayesian nonparametric models. Thus, the Gaussian process could be leveraged to regress the relationship between RSS measurement values and their corresponding locations. Furthermore,

Manuscript received March 5, 2020; revised April 30, 2020; accepted May 19, 2020. Date of publication May 21, 2020; date of current version November 12, 2020. This work was supported in part by NSF under Grant ECCS-1923163; and in part by the Wireless Engineering Research and Education Center and RFID Laboratory at Auburn University, Auburn, AL, USA. This article was presented in part at the IEEE Global Communications Conference, Abu Dhabi, UAE, December 2018. *(Xiangyu Wang and Xuyu Wang are co-first authors.) (Corresponding author: Shiwen Mao.)*

Xiangyu Wang and Shiwen Mao are with the Department of Electrical and Computer Engineering, Auburn University, Auburn, AL 36849 USA (e-mail: xzw0042@auburn.edu; smao@ieee.org).

Xuyu Wang was with the Department of Electrical and Computer Engineering, Auburn University, Auburn, AL 36849 USA. He is now with the Department of Computer Science, California State University, Sacramento, CA 95819 USA (e-mail: xuyu.wang@csus.edu).

Jian Zhang, Senthilkumar C. G. Periaswamy, and Justin Patton are with the RFID Laboratory, Auburn University, Auburn, AL 36849 USA (e-mail: jzz0043@auburn.edu; szc0089@auburn.edu; jbp0033@auburn.edu).

Digital Object Identifier 10.1109/JIOT.2020.2996564

the Gaussian process has the ability to accurately represent data when there is sufficient training data. However, this ability degrades dramatically when there is only sparse training data, which typically happens in RF fingerprinting. In fact, the Gaussian process is not effective at handling the nonstationary components of RSS samples due to the lack of fusion of kernels for dealing with complex training data [27]. Therefore, the Gaussian process could perform poorly with an unacceptable localization accuracy when it is trained with inadequate training data.

To address these challenges, we propose *DeepMap*, a *deep* Gaussian process-based system for indoor radio *map* construction and location estimation [28]. Like traditional fingerprinting-based methods, the DeepMap system includes an offline training stage and an online location estimation stage. In the offline stage, RSS samples, along with their corresponding location coordinates, are passed into a two-layer deep Gaussian process model that estimates the relationship between RSS values and location coordinates in a continuous space. In addition, we employ a Bayesian training method to maximize the marginal distribution of the observed RSS samples, to derive the optimal hyperparameters, where a variational lower bound is utilized to make the problem tractable. Unlike the Gaussian process, a deep Gaussian process is capable of constructing a precise radio map even with inadequate training data. The structural advantage of a deep Gaussian process enhances the learning capacity for training complicated data sets associated with abstract information [29]. Thus, the features of a small data set could be better captured by a deep Gaussian process when constructing radio maps.

In the online stage, we leveraged a Bayesian method to achieve high localization precision. The mobile device at an unknown location will collect new RSS samples from all the surrounding APs. With the radio maps generated by the deep Gaussian process, the estimated location of the mobile device can be obtained by using maximum *a posteriori* (MAP) estimation. Although the original DeepMap system is implemented with WiFi [28], this method is not restricted to use with only WiFi RSS values. It could be applied in systems using other types of wireless signals, such as RF identification (RFID) and Bluetooth low energy (BLE).

The main contributions made in this article can be summarized as follows.

1) We propose the DeepMap system that is the first, to the best of our knowledge, to use a deep Gaussian process model for radio map construction and indoor localization, and that effectively overcomes the drawbacks of the Gaussian process by generating detailed radio maps using sparse training data.
2) We design a two-layer deep Gaussian process model to regress the relationship between RSS samples and location, a Bayesian training method that optimizes model parameters, and a Bayesian fusion method that boosts localization performance.
3) We validate the performance of the proposed DeepMap system in two indoor environments with various levels of data availability and comparison with baseline schemes.

In the following, we discuss related works in Section II and present the preliminaries and motivates in Section III. The DeepMap design and analysis are introduced in Section IV, and the performance study is presented in Section V. Conclusions are given in Section VI.

II. Related Work

Recently, various indoor localization systems have been devoted to promoting localization precision with advanced methods and algorithms. In this section, we review the fingerprinting-based indoor localization systems and discuss two classes of fingerprinting-based systems that are closely related to DeepMap, i.e., 1) deep-learning-based systems and 2) radio map-based systems.

The first RSS-based fingerprinting system, RADAR [12], localized a target by comparing the fingerprints collected during the online stage to the saved RSS fingerprints using a deterministic method. To improve localization precision, Horus [13] leveraged a K-nearest-neighbor-based probabilistic method. However, the nature of RSS restricts the performance of RSS-based systems. First, the RSS values are significantly influenced by the multipath and shadow fading effects. Thus, due to the diversity of RSS, two consecutive RSS readings collected at the exact same location could be very different. Second, the RSS value is coarse information. Useful channel information could be easily lost. Compared to RSS, CSI is more fine-grained and depicts the characteristics of each subcarrier. FIFS [30] and PinLoc [31] utilized CSI to build fingerprints. The experimental results showed that both FIFS and PinLoc outperformed Horus. Although these fingerprinting-based systems had agreeable localization precision, the enormous fingerprint databases they require limited their application on mobile devices with limited storage.

Deep-learning-based indoor localization systems rely on deep neural networks to learn location features from CSI and use these features as fingerprints. DeepFi [14], [32] was the first work to use an autoencoder to extract features from CSI. DeepFi utilized the bias and weights from a well trained, three-layered autoencoder as fingerprints. PhaseFi [15], [33] and DFLAR [34] proposed to train the autoencoder with the phase values and images generated by CSI. Bi-modal CSI data was utilized in the BiLoc system [16] with an autoencoder for improved location performance. Additionally, WiDeep [35] improved the robustness of localization estimation by combining a stacked denoising autoencoder deep learning model with a probabilistic framework. Furthermore, Youssef and Agrawala [36] and Wang *et al.* [34] contributed to device-free indoor localization improvement with deep autoencoder networks. Due to the strong abilities of the convolutional neural network (CNN) in fields such as computer vision, it has been used to improve the performance of indoor localization systems. For example, a 6-layer CNN was employed in CiFi [17], [18]. In contrast to previous fingerprinting-based systems, CiFi did not use the fingerprinting database in the online stage and only stored a set of weights and biases for localization. Alternatively, Shao *et al.* [37] contributed to improving localization precision by preventing the "overfitting

problem" with a limited training data set. ResLoc [19] utilized a deep residual network to obtain submeter-level accuracy using a single AP.

However, due to the nature of fingerprinting-based systems, the localization problem was treated as a matching problem or multiclassification problem. Therefore, the density of fingerprints was closely related to the performance of the fingerprinting-based localization system. To address these problems, He and Chan [21] and Kumar *et al.* [38] generated radio maps for an indoor environment with a Gaussian process, which modeled the RSS values in a continuous space. By producing interpretable radio maps, researchers provided solutions to the existing fingerprinting-based localization problem. For example, WinIPS [39] leveraged GPR with polynomial surface fitting mean to predict RSS with virtual reference points. It overcame the laborious fingerprint collection effort in the offline phase and updated the radio map automatically in a dynamic environment. DncIPS [40] presented the FWA-GPR algorithm based on GPR and a fireworks algorithm (FWA). It was robust to environmental changes. However, the AP locations were not essential in DncIPS, which helped to improve its flexibility. Although both WinIPS and DncIPS solved the problem of updating fingerprints in a dynamic environment, their localization precision was not comparable to other deep-learning-based localization systems.

III. Preliminaries and Motivation

As a kernel-based Bayesian model, the Gaussian process has been successfully applied to solve regression and classification problems [27]. With the help of the Gaussian process, the uncertainty in input data distributed over a continuous space could be measured. Generally, a Gaussian process could be delineated by its covariance and mean function, which is a generalization of a multivariate Gaussian distribution.

For issues with radio map construction, we could treat measured RSS samples and the corresponding locations as a GPR model, that is

$$s(x) = f(x) + \epsilon \tag{1}$$

where $s(x)$ is the measured RSS sample at location x, $f(x)$ represents the pure RSS at location x, and ϵ is the observation noise, which follows an independent, identically distributed (i.i.d.) Gaussian distribution with zero mean and variance σ_n^2. The Gaussian process model assumes that the RSS measurements s_p and s_q at two different positions x_p and x_q, respectively, follow a joint Gaussian distribution with covariance $k(x_p, x_q)$, which is a kernel function for the two locations given by

$$k(x_p, x_q) = \sigma_f^2 \exp\left(-\frac{1}{2l^2}\left|x_p - x_q\right|^2\right) \tag{2}$$

where σ_f and l are the hyperparameters. Specifically, σ_f^2 represents the variance and l is a length scale, both of which describe the smoothness of the kernel function. The predicted RSS for an unknown position x_* can be obtained by

$$\Pr(f(x_*)|X, Z, x_*) = N\left(f(x_*); u_*, \sigma_*^2\right) \tag{3}$$

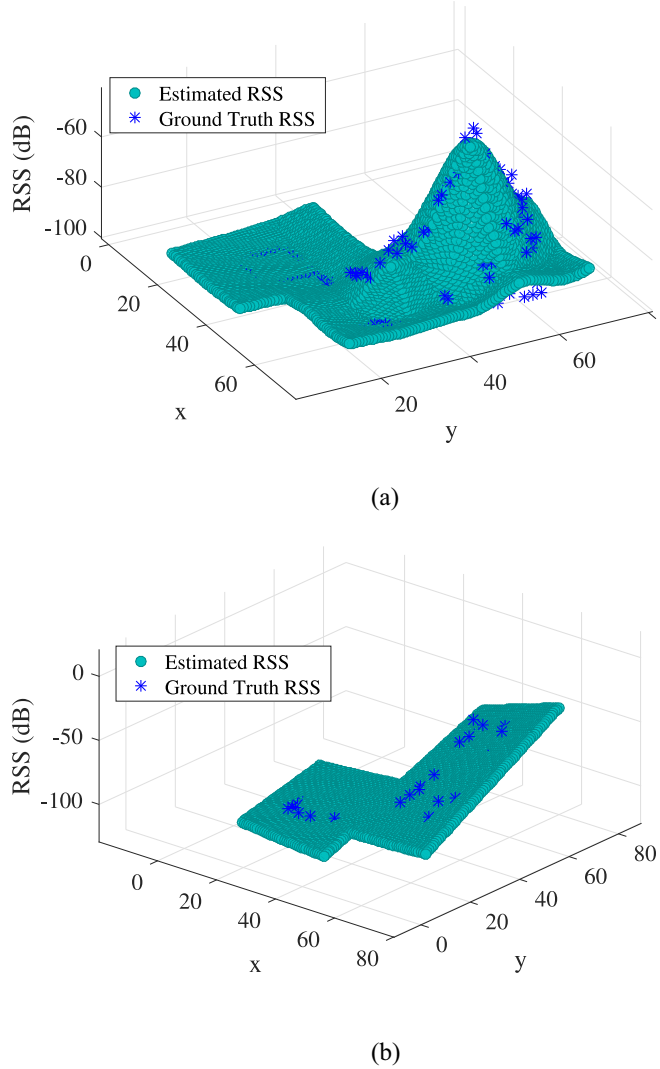

Fig. 1. RSS radio maps constructed using the Gaussian process model using different amount of training data. (a) Using 100% training data. (b) Using 20% training data.

$$u_* = k_*^T\left(K + \sigma_n^2 I\right)^{-1} Z \tag{4}$$

$$\sigma_*^2 = k(x_*, x_*) - k_*^T\left(K + \sigma_n^2 I\right)^{-1} k_* \tag{5}$$

where k_* is an $n \times 1$ vector of covariances between training locations X and x_*, K is the covariance matrix of training locations X, and Z is a matrix of training observation values. In addition, the hyperparameters σ_f and l can be estimated by a maximum-likelihood approximation method.

We use the Broun Hall data set (see Section V-A) collected on the third floor of Broun Hall in the Auburn University campus as an example. The RSS radio maps constructed by Gaussian process models using the Broun Hall data set are shown in Fig. 1(a). We utilized all the samples in the Broun Hall data set to train the Gaussian process model. Obviously, the bell-shaped RSS radio map is consistent with most ground-truth RSS measurements. Thus, this example verifies that a Gaussian process could model the distribution of RSS values in an indoor environment and regress the relationship with adequate training data. However, the ability of the Gaussian

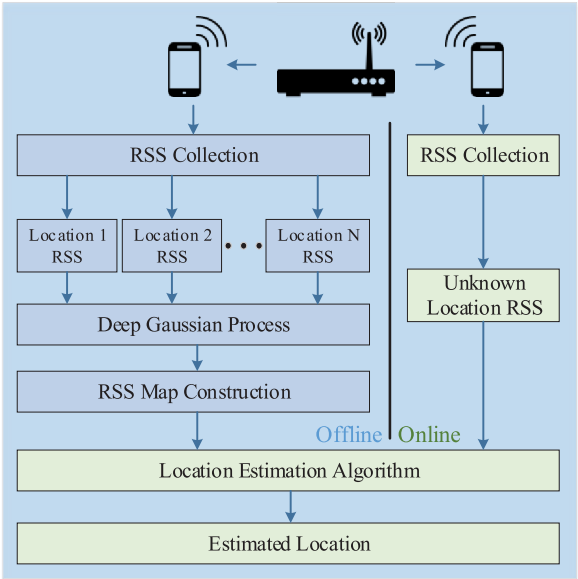

Fig. 2. DeepMap system architecture.

process to depict RSS data distributions degrades when there is inadequate training data. Fig. 1(b) plots an RSS radio map constructed with 20% of the training data in the Broun Hall data set using the Gaussian process. We find that the RSS radio map in Fig. 1(b) is flat and lacks details. Clearly, most of the variations in Fig. 1(a) are lost in Fig. 1(b), although the upper right corner is still the highest position in Fig. 1(b). In other words, the nonstationary components of RSS values are lost during radio map construction by the Gaussian process model, due to the lack of fusion of kernels in the complex input data set. Therefore, this coarse RSS radio map is the result of a deficiency of the Gaussian process that hampers high localization accuracy during the online stage. To address this problem, we propose a DeepMap system to construct RSS radio maps using *deep Gaussian process* models in Section IV.

IV. DeepMap System

A. DeepMap System Architecture

Fig. 2 presents the architecture of the DeepMap system. The DeepMap system is a fingerprinting-based indoor localization method that consists of two stages: 1) the offline training stage and 2) the online location estimation stage. In the offline stage, we recorded the RSS samples from training positions along with their corresponding location coordinates. For each training location, RSS measurements are collected from as many available APs as possible to enhance localization accuracy. To guarantee that the RSS records from all the training locations are of the same size, we collect all potential RSS readings (i.e., from all the APs). If the RSS for a specific AP is not detected, the corresponding RSS reading will be set to −99 dBm. This way, a training data set will be generated with RSS records and their corresponding location labels. To construct the RSS radio map of an indoor environment, we used a deep Gaussian process to regress the training data set. The well-trained model (a constructed map) describes the relationship between RSS samples and location labels in a continuous space. This radio map will be used for location estimation in the online stage.

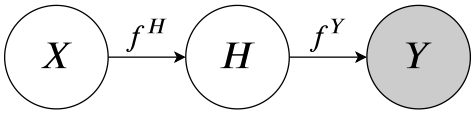

Fig. 3. Deep Gaussian process model for RSS radio map construction.

In the online stage, we collect new RSS samples using the mobile device at an unknown location and contrast the new RSS samples with the RSS samples in the constructed radio map. When we determine the similarities between the measured RSS values and the recorded RSS values from the radio map, we will be able to infer the location of the mobile device using a Bayesian fusion method.

Unlike traditional fingerprinting methods, which save the original RSS samples as fingerprint [12], [13], or the previous autoencoder-based methods, which use a bunch of well-trained weights as fingerprint [14]–[16], [33], the DeepMap system incorporates two different storage strategies. Depending on each mobile device's specifications, DeepMap allows users to store the model at an edge device or in the cloud, and use it to estimate location in the online stage if storage space is limited. Alternatively, the constructed radio maps can be saved at the mobile device to accelerate the localization process. Furthermore, the resolution of the constructed radio maps can be adaptive. In fact, a high-resolution map offers high localization precision at the cost of localization speed, while a low-resolution map achieves a coarse precision but also fast localization. In the following sections, we will show that satisfactory localization results can be achieved by the proposed DeepMap system even with a low-resolution map.

B. Deep Gaussian Process for Radio Map Construction

We propose a deep Gaussian process model for radio map construction using WiFi RSS samples. This process is represented by a graphical model with three different layers of nodes, including the leaf nodes, the intermediate latent nodes, and the parent nodes [29]. The model is illustrated in Fig. 3. For radio map construction, the leaf nodes represent RSS samples, denoted by $Y \in \Re^{N\times D}$, where N and D are the number of training locations and the number of APs, respectively. The intermediate latent nodes are denoted by $H \in \Re^{N\times Q}$, where Q is the number of the intermediate latent nodes in this layer. These latent nodes are not observable in the training stage. For the DeepMap system, we adopt one intermediate latent layer to obtain a deep Gaussian process model. The parent nodes are denoted by $X \in \Re^{N\times M}$, where M is the size of input data. For radio map construction, the parent nodes X represent the training locations.

Our proposed deep Gaussian process model for radio map construction is a generative model for regression. This generative process can be formulated as

$$h_{nq} = f_q^H(x_n) + \epsilon_{nq}^H, \quad q = 1, 2, \ldots, Q, \quad x_n \in \Re^M \tag{6}$$

$$y_{nd} = f_d^Y(h_n) + \epsilon_{nd}^Y, \quad d = 1, 2, \ldots, D, \quad h_n \in \Re^Q \tag{7}$$

where $f^H \sim GP(\mathbf{0}, k^H(X, X))$ and $f^Y \sim GP(\mathbf{0}, k^Y(H, H))$ are Gaussian processes, and the latent nodes H connect them. Note that these two processes only depend on the covariance function k for different inputs, which is chosen to be the automatic relevance determination (ARD) covariance function, given by

$$k(x_i, x_j) = \sigma^2 \exp\left(-\frac{1}{2}\sum_{q=1}^{Q} w_q (x_{i,q} - x_{j,q})^2\right) \tag{8}$$

where σ is the hyperparameter and w_q is the weight for latent node q. Irrelevant dimensions can be removed by setting their weights to zero.

C. Offline Bayesian Training

The objective of Bayesian training is to maximize the marginal distribution of observed RSS values Y to determine the optimal hyperparameters, which is formulated as

$$\max \ \log p(Y) = \log \int_{X,H} p(Y|H)p(H|X)p(X). \tag{9}$$

Because of the nonlinear functions for H and Z, it is difficult to solve the integral in (9) using the maximum-likelihood method. In DeepMap, we apply Jensen's inequality to find a variational lower bound for this marginal distribution, denoted by $\mathcal{L} \leq \log p(Y)$ and given by

$$\mathcal{L} = \int_{F^Y, H, F^H, X} Q \cdot \log\left(\frac{p(Y, F^Y, H, F^H, X)}{Q}\right) \tag{10}$$

where Q is the variational distribution. F^H is the collection of latent function instantiations, which has a normal distribution given by

$$F^H = \left\{f_q^H\right\}_{q=1}^{Q}, \ \ f_{nq}^H = f_q^H(x_n). \tag{11}$$

Similarly, F^Y is given by

$$F^Y = \{f_d^Y\}_{d=1}^{D}, \ \ f_{nd}^Y = f_d^Y(h_n). \tag{12}$$

The term $p(Y, F^Y, H, F^H, X)$ is given by

$$\begin{aligned} p(Y, F^Y, H, F^H, X) &= p(Y|F^Y) \cdot p(F^Y|H) \cdot p(H|F^H) \\ &\quad \times p(F^H|X) \cdot p(X). \end{aligned} \tag{13}$$

However, integral (10) is still intractable due to the nonlinearity in both $p(F^Y|H)$ and $p(F^H|X)$. Consider the probability space with K auxiliary pseudoinputs $\bar{H} \in \Re^{K\times Q}$ and $\bar{X} \in \Re^{K\times M}$ [41], whose function values are $U^Y \in \Re^{K\times D}$ and $U^H \in \Re^{K\times Q}$, respectively. Then, we derive the augmented probability space as

$$\begin{aligned} &p(Y, F^Y, H, F^H, X, U^Y, U^H, \bar{H}, \bar{X}) \\ &\quad = p(Y|F^Y) \cdot p(F^Y|U^Y, H) \cdot p(U^Y|\bar{H}) \\ &\qquad \times p(H|F^H) \cdot p(F^H|U^H, X) \cdot p(U^H|\bar{X}) \cdot p(X). \end{aligned} \tag{14}$$

To remove the nonlinear items $p(F^Y|U^Y, H)$ and $p(F^H|U^H, X)$, the variational distribution Q can be defined as follows:

$$\begin{aligned} Q &= p(F^Y|U^Y, H) \cdot q(U^Y|\bar{H}) \cdot q(H) \\ &\quad \times p(F^H|U^H, X) \cdot q(U^H|\bar{X}) \cdot q(X) \end{aligned} \tag{15}$$

where $q(U^Y|\bar{H})$ and $q(U^H|\bar{X})$ are free-form variational distributions, and $q(H)$ and $q(X)$ are both Gaussian.

According to (13) and (15), we update the variational lower bound in (10) as

$$\mathcal{L} = \int Q \log\left(\frac{p(Y|F^Y)p(U^Y|\bar{H})p(H|F^H)p(U^H|\bar{X})p(X)}{q(U^Y|\bar{H})q(H)q(U^H|\bar{X})q(X)}\right)$$

where the integration is with respect to $\{F^Y, H, F^H, X, U^H, U^Y\}$. By grouping the variables for Y and H, respectively, we can rewrite the variational lower bound as

$$\mathcal{L} = s_Y + s_H - q(H) \cdot \log(q(H)) - \mathrm{KL}(q(X)||p(X)) \tag{16}$$

where KL is the Kullback–Leibler divergence [42], s_Y is calculated by

$$s_Y = \mathbb{E}_{p(F^Y|U^Y,H)q(U^Y|\bar{H})q(H)}\left(\log p(Y|F^Y) + \log\frac{p(U^Y|\bar{H})}{q(U^Y|\bar{H})}\right) \tag{17}$$

and s_H is calculated by

$$s_H = \mathbb{E}_{p(F^H|U^H,X)q(U^H|\bar{X})q(X)}\left(\log p(H|F^H) + \log\frac{p(U^H|\bar{X})}{q(U^H|\bar{X})}\right). \tag{18}$$

It can be seen that both s_Y and s_X are Gaussian densities, and are thus tractable. In fact, Bayesian training for a deep Gaussian process can maximize the variational lower bound $\mathcal{L}$ to find the suboptimal hyperparameters, inducing points (i.e., $\bar{H}$ and $\bar{X}$), and variational parameters [29].

We use the same Broun Hall data set as an example of the proposed method. The constructed RSS radio map shown in Fig. 4(a) is generated by a deep Gaussian process with 100% training data in the Broun Hall data set. Although a similar bell-shaped surface is created by the Gaussian process [see Fig. 1(a)], our proposed deep Gaussian process produces more details that help to improve localization precision. For example, the slight fluctuations close to the coordinate's origin is captured by the deep Gaussian process model in Fig. 4(a). However, the corresponding area in Fig. 1(a) tends to be a flat surface, which is constructed by the Gaussian process model. In Fig. 4(b), the RSS radio map is constructed by the deep Gaussian process model using only 20% of the training data. Clearly, a bell-shaped surface is maintained similarly as in the radio map generated using 100% training data, even though only 20% of the training data is utilized. Additionally, the surface contains many nonlinear characteristics.

From this comparison example of the Gaussian process and deep Gaussian process models, it is safe to say that the deep Gaussian process model can handle nonstationary components, in contrast to the detail-less surfaces constructed by the Gaussian process model in Fig. 1. Moreover, nonlinear characteristics are also reproduced with only minimal training data because the deep Gaussian process has a deep and heterogeneous nonlinear structure that is more effective for complex training data. Thus, WiFi RSS radio maps constructed by the deep Gaussian process model capture more detailed information about the distribution of real RSS samples in

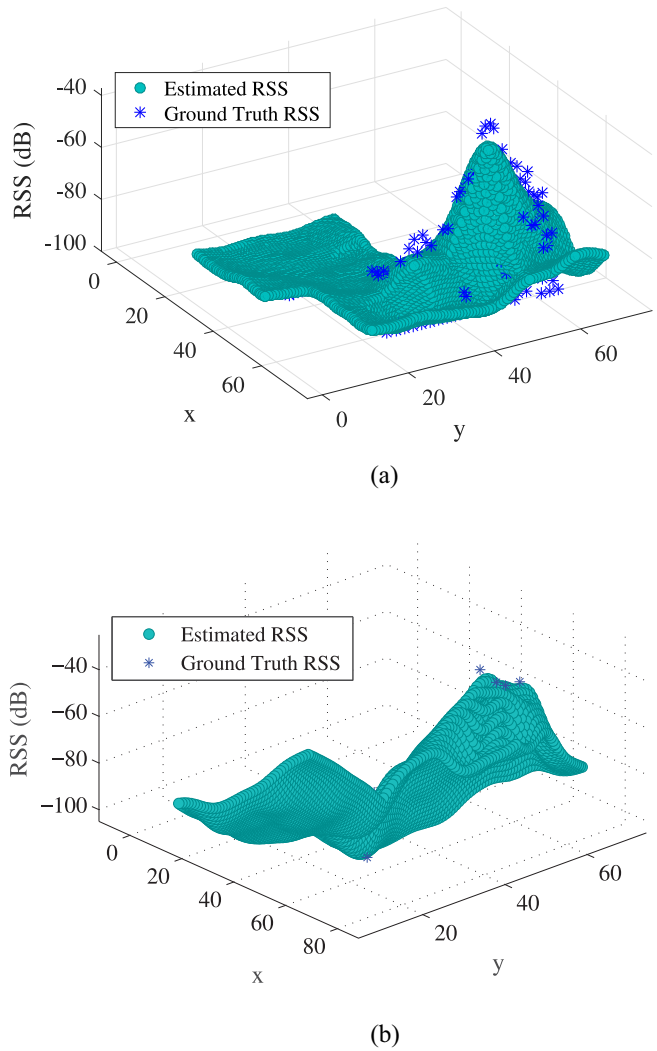

Fig. 4. RSS radio map constructed using the deep Gaussian process model using different amount of training data. (a) Using 100% training data. (b) Using 20% training data.

indoor environments, which considerably contributes toward improving localization precision.

D. Online Location Estimation

In the online localization stage, we use a Bayesian method to estimate the location of a mobile device using newly measured RSS samples from totally D APs and the constructed radio maps obtained in the offline stage. We discretize the continuous RSS radio map to obtain T reference positions. The size of T is dependent upon the resolution of the RSS radio map.

The pseudocode for online location estimation is presented in Algorithm 1. The input to Algorithm 1 is the newly measured RSS values v_j and the constructed radio map r^j for each AP j, and the total number of APs D. We have $T = |r^j|$. In the DeepMap system, we assume that the likelihood function $p(v_j|l_i)$ is a Gaussian function. Thus, the similarity between the measured RSS value v_j and the data $r^j_{l_i}$ at location l_i from

Algorithm 1 Pseudocode for Online Location Estimation

Input: the newly measured RSS samples v_j and the constructed radio map r^j for each AP j, the total number of APs D;

Output: the estimated location $\hat{l}$;

1: //j denotes the index of APs
2: //i represents the index of reference points in radio map r^j
3: **for** $j = 1 : D$ **do**
4: **for** $i = 1 : T = |r^j|$ **do**
5: //compute the likelihood function $p(v_j|l_i)$
6: $p(v_j|l_i) = \exp\left(-\frac{1}{\lambda\sigma^2}\left\|v_j - r^j_{l_i}\right\|\right)$;
7: **end for**
8: //compute the posterior probability $p(l_i|v_j)$
9: $p(l_i|v_j) = \frac{p(v_j|l_i)}{\sum_{k=1}^{T} p(v_j|l_k)}$;
10: **end for**
11: //derive the location of the mobile device using MAP estimation
12: $\hat{l} = \text{argmax}_{\{l_1,l_2,\ldots,l_T\}}\left(\prod_{j=1}^{D} p(l_i|v_j)\right)$;
13: **return** $\hat{l}$.

AP j is computed in step 6 [14]. Here, σ^2 is the variance and λ is the parameter of the variance of input RSS samples.

Based on the likelihood function, the posterior probability $p(l_i|v_j)$ for AP j can be obtained by

$$p(l_i|v_j) = \frac{p(l_i)p(v_j|l_i)}{\sum_{k=1}^{T} p(l_k)p(v_j|l_k)} \tag{19}$$

where $p(l_i)$ is the prior probability for the device placed at position l_i. Generally, $p(l_i)$ is assumed to have a uniform distribution over the T reference positions. Therefore, the posterior probability $p(l_i|v_j)$ is obtained in step 9, as

$$p(l_i|v_j) = \frac{p(v_j|l_i)}{\sum_{k=1}^{T} p(v_j|l_k)}. \tag{20}$$

Additionally, we assume that the posterior probability $p(l_i|v_j)$ is independent for each AP. Consequently, we derive the location of the mobile device using MAP estimation as follows (see step 12):

$$\hat{l} = \underset{\{l_1,l_2,\ldots,l_T\}}{\text{argmax}}\left(\prod_{j=1}^{D} p(l_i|v_j)\right). \tag{21}$$

V. Experimental Study

A. Experiment Methodology

For this article, we prototype the DeepMap system with commodity WiFi devices to evaluate its localization performance. Three baseline schemes are implemented and evaluated for comparison purpose. The first one, termed "Gaussian process," is implemented by replacing the deep Gaussian process model with a Gaussian process model [38], while keeping all other parts the same. The RADAR [12] and Horus [13] are the two other baseline schemes we implemented for comparison purpose. Both RADAR and Horus

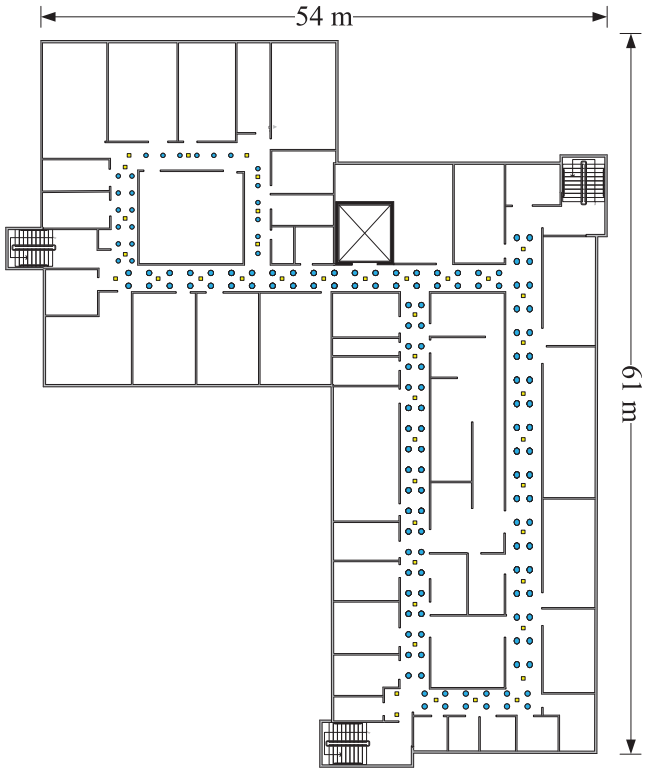

Fig. 5. Layout of the third floor of Broun Hall at Auburn University: training locations are marked as blue dots and testing locations are marked as yellow squares.

are representative RSS-based fingerprinting schemes, while RADAR uses a deterministic scheme and Horus utilizes a K-nearest-neighbor bases probabilistic method for location estimation. To limit bias, all the schemes are executed using the same Broun Hall and public data sets; thus, the training data and test data for the schemes are identical. Additionally, the same online location estimation algorithm presented in Section IV-D is used for DeepMap and Guassian process schemes to ensure consistency.

First, we evaluate DeepMap's performance with the Broun Hall data set (collected from the third floor of Broun Hall at Auburn University). In this scenario, we use Wi-Fi Scanner 3.4 to collect RSS measurements in the offline and online stages within a surveillance area of about 2300 m^2. The floor plan is shown in Fig. 5, where 157 locations are included in the training data set (represented by blue dots). The space between each blue dot is 2 m. The test data are gathered from 43 locations, each represented by a yellow square, and the space between yellow squares was 4 m. In this data set, the RSS values are gathered from 433 APs (for the four-layer building), which consists of both 5-GHz APs and 2.4-GHz APs from various manufacturers. Furthermore, the RSS values for out-of-range APs are set to -99 dBm, as discussed.

Additionally, we also tested the DeepMap system using a public data set to examine its localization performance [43]. The experimental area is approximately 860 m^2 and includes eight classrooms, four offices, and a main hallway. The floor plan is shown in Fig. 6. Similar to the Broun Hall data set,

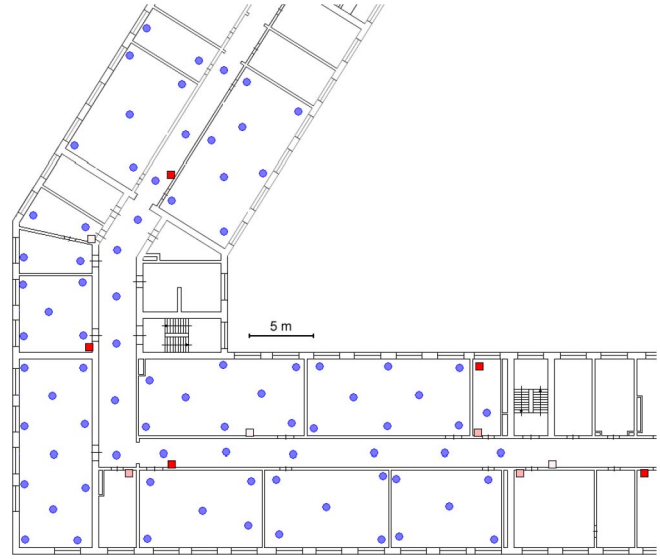

Fig. 6. Layout of the public data set from [43]: blue dots denote the training positions, red squares are APs on the fifth floor, orange squares are APs on the fourth floor, and white squares are the APs on the third floor (figure courtesy [43]).

the RSS measurements in the public data set are also collected from APs deployed on multiple floors. In the public data set layout, blue dots denote the training positions, red squares are APs on the fifth floor, orange squares are APs on the fourth floor, and white squares are the APs on the third floor. All RSS values in the data set are collected from both 5-GHz APs and 2.4-GHz APs. The training data is collected for 82 locations, and the test data set includes RSS values from 34 locations (their coordinates are known as ground truth, but are not shown in the figure). The distance between two adjacent locations is 2.6 m. In the online localization stage, new RSS samples are collected for every testing location twice, each time facing a different direction.

B. Accuracy of Location Estimation

1) Comparison With Gaussian Process: First, we confirmed the localization accuracy with adequate training data. Fig. 7 illustrates the cumulative distribution function (CDF) of localization errors for the proposed DeepMap system and the Gaussian process-based baseline scheme. In both schemes, we use all the RSS samples in the Broun Hall data set to train the models. For DeepMap, the median localization error is 1.3 m, and the Gaussian process-based scheme obtains a median error of 1.5 m. This comparison shows that DeepMap is more accurate than the Gaussian process-based scheme. Additionally, 60% of the localization errors are lower than 2 m for the Gaussian process, whereas 75% of the localization errors are lower than 2 m with DeepMap. Furthermore, the Gaussian process's largest error is 6.182 m, which is greater than DeepMap's largest error of 5.207 m. Thus, DeepMap outperforms the Gaussian process-based scheme with respect to localization accuracy, when adequate training data is available.

Similarly, Fig. 8 shows the localization performance of both schemes using the public data set [43]. When we use the

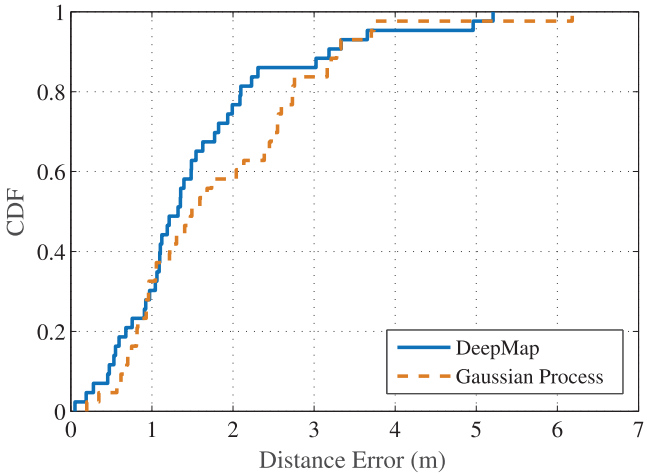

Fig. 7. CDF of localization errors for the proposed DeepMap system and the Gaussian Process-based scheme when 100% of the training data in the Broun Hall data set is used.

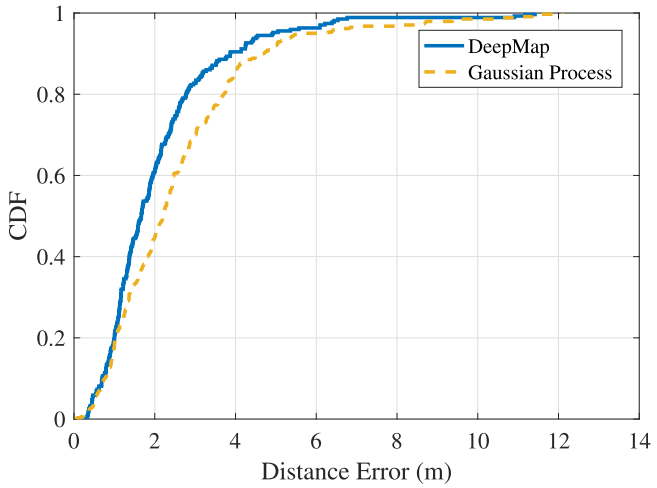

Fig. 8. CDF of localization errors for the proposed DeepMap system and the Gaussian Process-based scheme when 100% of the training data in the public data set is used.

public data set to train these two algorithms, the median errors for DeepMap and Gaussian process are 1.668 and 2.2017 m, respectively. Again, DeepMap achieves a better localization accuracy than the Gaussian process-based scheme in this environment. For DeepMap, we also note that more than 80% errors are under 2.8 m; however, only 65% test points for the baseline scheme could reach this same level of accuracy. Therefore, for the experiment using the public data set, DeepMap also outperforms the Gaussian process-based scheme when the entire training data set is available.

Additionally, we evaluated the performance of both schemes using only a fraction of the training data. In Fig. 9, we plot the mean distance errors achieved by the two schemes when different percentages of training data in the Broun Hall data set are used. Regarding the Broun Hall data set experiment, the mean distance error is 1.569 m when all fingerprints are used. However, when 90% training data are used by DeepMap, the minimum mean distance error 1.536 m is reached. We also find that distance errors are robust to changes in the

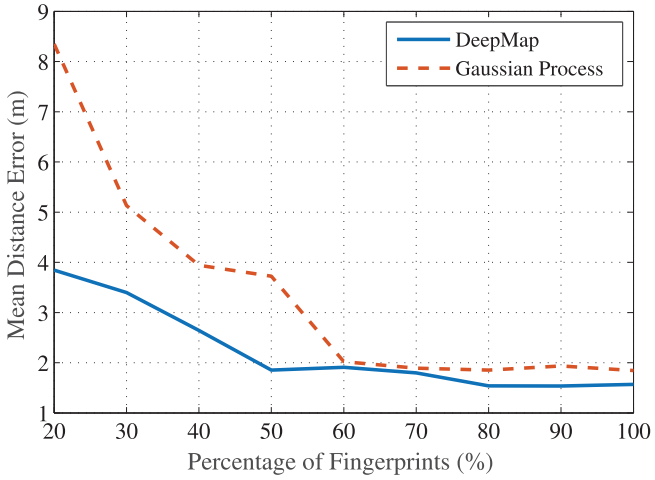

Fig. 9. Mean localization errors for the proposed DeepMap system and the Gaussian Process-based scheme using different percentages of training data in the Broun Hall data set.

percentage of samples when more than 50% fingerprints are available to DeepMap. The Gaussian process achieves its best performance, 1.845 m, when all the training data are available. Regardless, this value is greater than the lowest mean distance error for DeepMap. Although the Gaussian process's mean distance errors are robust when more than 60% samples are available, the distance error increases dramatically to 3.725 m when 50% of samples are used. Additionally, the Gaussian process mean distance error increases further to 8.3496 m when 20% of fingerprints are used to train the model. The distance error for our DeepMap system does not change such abruptly; its largest distance error is 3.8447 m when 20% of fingerprints are utilized to train the model. Note that in Fig. 9, all errors obtained by DeepMap are lower than the corresponding errors achieved by the Gaussian process-based scheme.

Furthermore, we conduct similar experiments using the public data set. In Fig. 10, minimum distance errors of 2.12 m for DeepMap and 2.489 m for the Gaussian process are obtained when all training data are available. However, distance error for the Gaussian process-based approach increases dramatically with a decrease in the available training data. With only 20% training data available to the Gaussian process-based scheme, the maximum distance error is 11.67 m. Both methods show larger errors when the algorithms are trained with only 20% data, but the maximum error produced by DeepMap is about half of that of the Gaussian process-based scheme. However, the performance of DeepMap is improved significantly when at least 40% samples are used to train the algorithm. For example, at 40% data availability, the mean distance error for DeepMap becomes 3.892 m, which is similar to the performance of the Gaussian process-based scheme when 70% of public data is available. Thus, DeepMap exhibits a more robust performance with incomplete training data sets.

In conclusion, when there is sufficient training data, both DeepMap and the Gaussian process-based scheme are able to regress the outline of the RSS surface. However, more detailed maps are generated by DeepMap than by the baseline scheme.

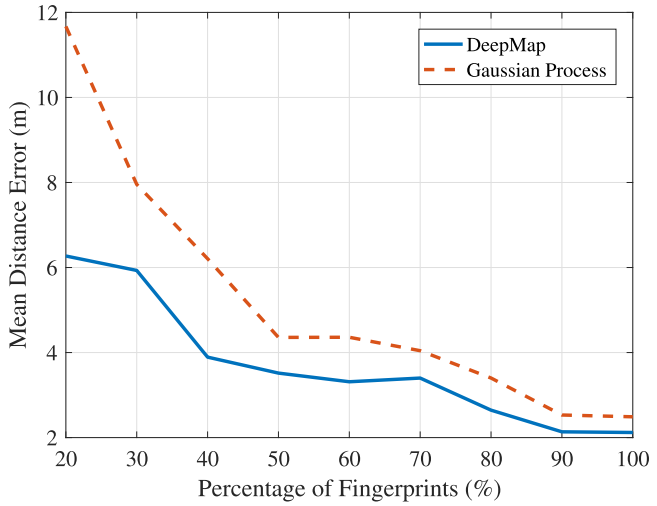

Fig. 10. Mean localization errors for the proposed DeepMap system and the Gaussian Process-based scheme using different percentages of training data in the public data set.

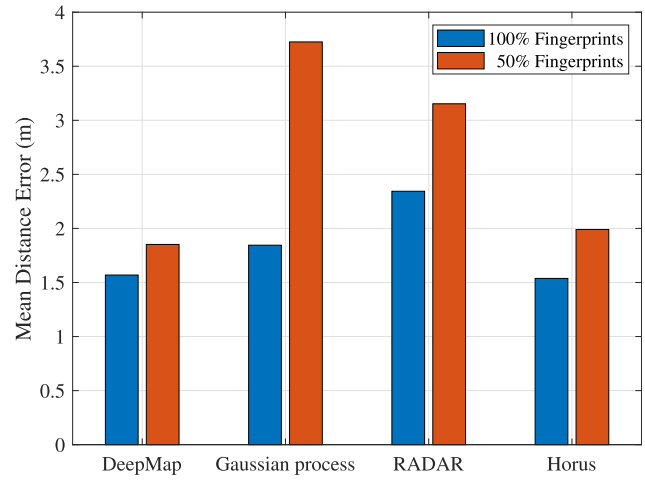

Fig. 11. Mean localization errors for the Broun Hall data set using different percentages of fingerprints.

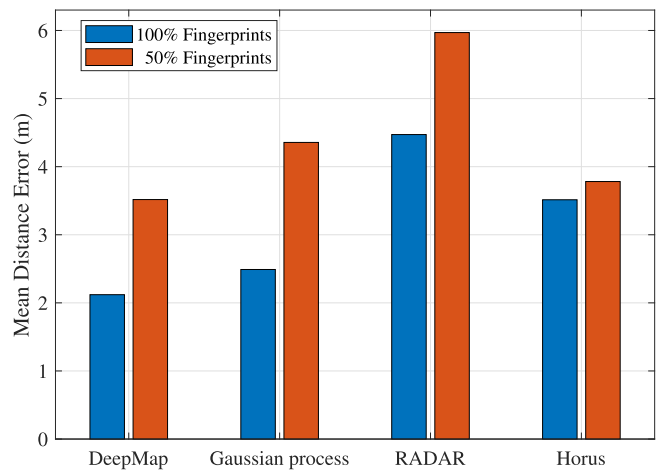

Fig. 12. Mean localization errors for the public data set using different percentages of fingerprints.

Regarding the map constructed by the Gaussian process-based scheme, it does not contain much detail, such as nonstationary components, and thus, the minimum error is slightly greater than that produced by DeepMap. When only limited amounts of RSS training samples are available, the localization error of the Gaussian process-based scheme increases dramatically, while DeepMap is more robust to this change. Additionally, nonlinear characteristics are captured by DeepMap even with few available RSS samples. Thus, DeepMap achieves higher localization accuracy and is more robust than the Gaussian process-based baseline scheme.

2) Comparison With RADAR and Horus: For more comparisons, we also evaluate the performance of two existing localization methods, RADAR and Horus, using the Broun Hall data set and the public data set. Both methods have been introduced in Section II. Fig. 11 depicts the mean localization errors achieved by the four schemes using either 50% or 100% of fingerprints in the Broun Hall data set. We can see that the precision of Horus is comparable to the performance of DeepMap when all the fingerprints are leveraged to train the model. Furthermore, the localization error of RADAR is much higher than that of the other three methods. With 50% fingerprints, the localization precision of all the four methods degrades in varying degrees. The mean distance error of Horus increases from about 1.5 to 2.0 m, which is higher than the corresponding error of DeepMap. Moreover, Horus shows better performance than the Gaussian process when the training fingerprints are inadequate.

We present the mean distance errors for the public data set in Fig. 12. Overall, all the methods perform worse than with the Broun Hall data set. This is because the Broun Hall data set includes many more APs than the public data set. We note that DeepMap has the best accuracy no matter fingerprints are adequate or not. Even though the availability of fingerprints does not affect the precision of Horus significantly, its mean distance error is much higher than DeepMap when 100% fingerprints are utilized. Therefore, it is safe to say that DeepMap has the best accuracy among these localization methods, and it is sufficiently robust to deficiency of fingerprints.

C. Impact of Design Parameters

To investigate the impact of system parameters on the localization precision of DeepMap, we use all the RSS samples in the Broun Hall data set in the following experiments. In each experiment, we repeat the training process five times with identical parameter settings. We recorded the average test result and present it in the plots.

1) Impact of the Number of Inducing points: In the DeepMap system, K represents the number of inducing points. Although it could be different for every layer of the overall structure, we keep the number of inducing points the same in each layer to simplify this article. As is shown in Fig. 13, we compare the mean distance errors for different values of K. According to Fig. 13, the mean distance error gradually decreases along with the increase in K. After K is greater than 40, the impact of K on the mean distance error decreases and the mean distance error converges to 1.65 m. Fig. 14 depicts the corresponding training times for different values

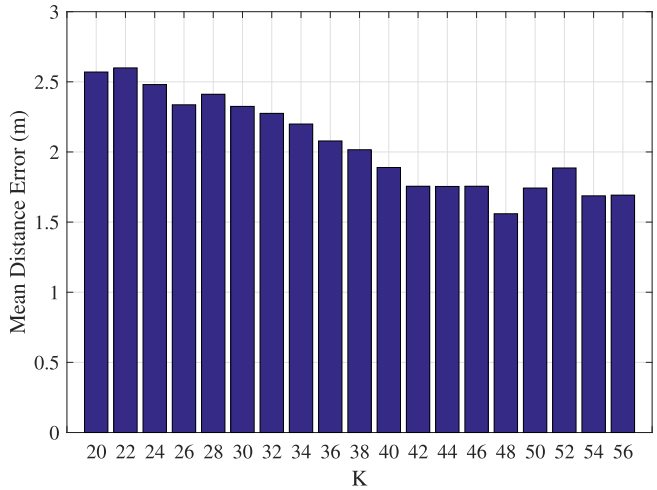

Fig. 13. Mean distance errors at different values of K.

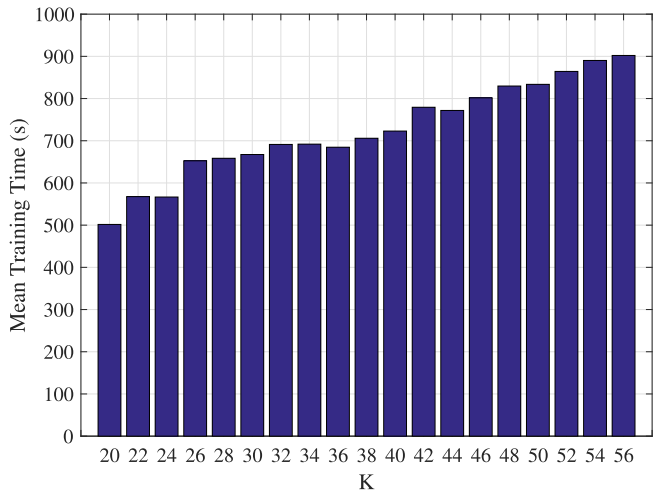

Fig. 14. Mean training times at different values of K.

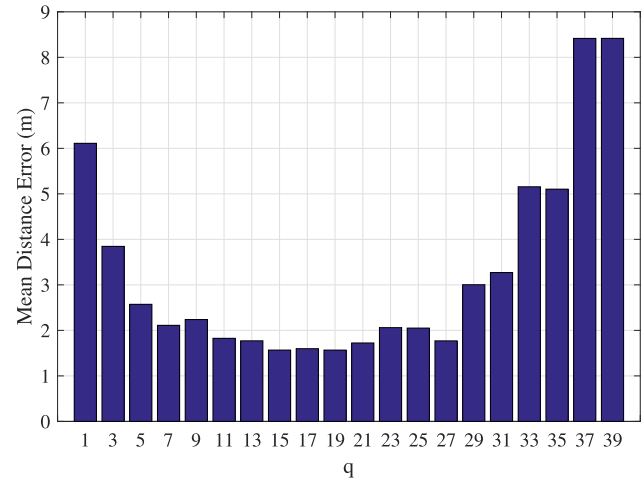

Fig. 15. Mean distance errors at different values of q.

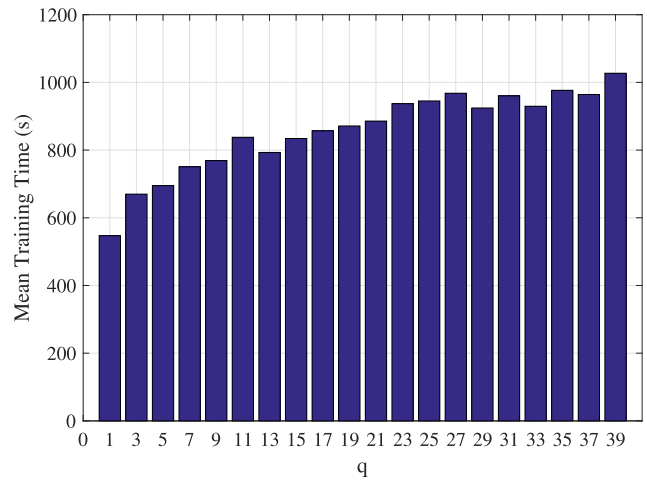

Fig. 16. Mean training times at different values of q.

of K. As shown, the mean training time increases along with the increase in K. Considering that the training time (in the offline stage) would not jeopardize the user experience in the online stage, K is set to 48 for obtaining the best localization performance in the following experiments.

2) Impact of the Number of Latent Nodes: The number of latent nodes in the deep Gaussian process is denoted by q. Ideally, each latent node would have its own weight w_q, but the node could also be removed by setting the weight to 0. We designed a specific experiment to evaluate the effect of q on the performance of our DeepMap system and to optimize the value of q that achieves the best localization precision. In this experiment, the value of K is set to 48 to eliminate its effect. Twenty different values of q are assessed with DeepMap to evaluate their effect on the performance of our system. For each q value, the training process was repeated five times to minimize randomness in the results.

Fig. 15 shows the mean distance errors as q is increased. As the number of latent nodes raises from 1 to 9, the mean distance error declines rapidly from about 6 m to about 2 m. When the value of q is between 11 and 27, the mean distance error does not fluctuate significantly. The lowest error is produced when q is between 15 and 19. When q becomes greater than 27, it produces a sharp rise in the mean distance error from 1.77 to 8.4 m. Therefore, we conclude that the localization precision of our DeepMap system could be degraded with an oversized q value, even though the weight for the excessive latent node could be set to zero. Additionally, we investigated the impact of q on the mean training time. The results are presented in Fig. 16. Similar to the impact of K, the mean training time goes up gradually with increases in q. To obtain the highest localization precision, we set q to 17 in the following experiments. Fig. 16 shows that the training time is only about 14 min when q is 17. Note that all the samples in the Broun Hall data set are utilized in this experiment. The training process would speed up if fewer samples are utilized; thus, the DeepMap system could react to the change of environment by updating the RSS samples and training the deep Gaussian process model in real time.

3) Impact of the Number of Iterations for Initializing the Variational Distribution: Fig. 17 plots the influence of the number of iterations performed for initializing the variational distribution on the localization precision of DeepMap. As

TABLE I
MAP CONSTRUCTION TIME, TESTING TIME, AND MAP SIZES AT DIFFERENT MAP RESOLUTIONS

Map Resolution (cm)	50	75	100	125	150	175	200	225	250	275	300	325	350	375	400
Map Construction Time (s)	24.3	9.38	5.08	3.13	2.11	1.56	1.24	0.95	0.77	0.63	0.53	0.46	0.40	0.33	0.33
Testing Time (s)	0.91	0.46	0.27	0.20	0.15	0.12	0.11	0.09	0.09	0.08	0.07	0.04	0.04	0.03	0.03
Map Size (MB)	12.4	5.52	3.17	2.03	1.38	1.03	0.83	0.64	0.51	0.44	0.36	0.31	0.27	0.22	0.21

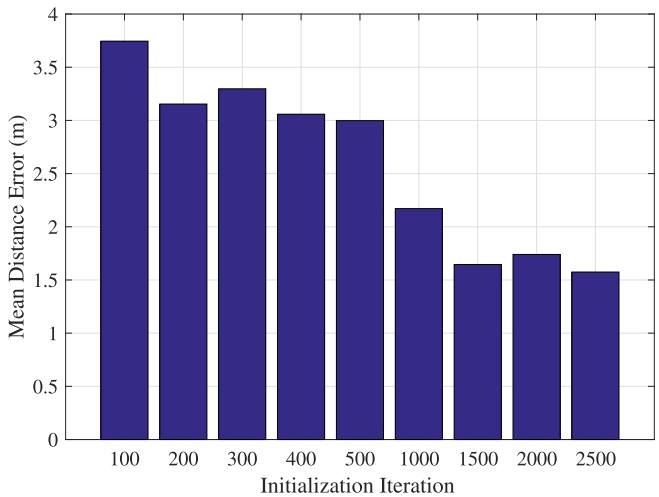

Fig. 17. Mean distance errors at different numbers of iterations for initializing the variational distribution.

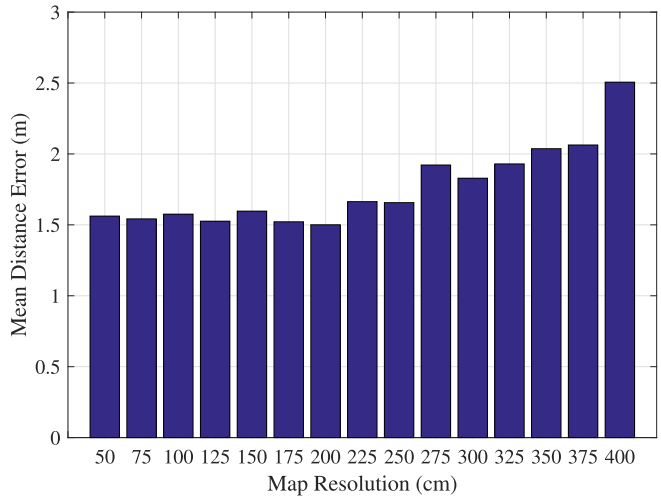

Fig. 18. Mean distance errors at different map resolutions.

shown in Fig. 17, the mean distance error drops slightly when the initialization iterations increase from 100 to 200. When initialization iterations range between 200 and 500, the localization precision remains stable and the mean distance error is about 3 m. To better assess the effect of initialization iterations on localization precision, we increased the initialization iteration number in steps of 500 in the rest of the experiments. With 1000 initialization iterations, the localization precision is improved significantly. When the number of initialization iterations reaches 1500, the mean distance error continued to decrease. However, the localization performance of DeepMap does not continue to improve once the number of initialization iterations becomes greater than 1500. Moreover, the mean distance error remains at the level around 1.6 m.

4) Impact of the Resolution of Constructed Radio Map: Fig. 4 depicts the reconstructed RSS radio map that was generated by 100% of fingerprints in the Broun Hall data set, where the green dots represent the reconstructed RSS values at various reference positions. The resolution of the reconstructed RSS radio map is decided by the density of the reference points. To investigate the impact of map resolution on the performance of the DeepMap system, we generate 15 maps with different resolutions using the well-trained deep Gaussian process model. As shown in Fig. 18, localization precision is not significantly affected by map resolution when the resolution is higher than 200 cm. Additionally, Table I shows that the size of the RSS radio map shrinks rapidly when map resolution is decreased from 50 to 200 cm. Thus, a fine-grained RSS radio map is not essential for the improved performance of the DeepMap system. However, mean distance error gets larger if the map resolution is further decreased. The worst localization precision is obtained with the map resolution of 400 cm.

According to Table I, map size and time of map construction are correlated to the map's resolution. When the map resolution is 50 cm, the mean distance error is 1.5 m, but the RSS radio map would be enormous and cost a mobile device 12.4 MB in storage. Correspondingly, testing and map construction times are also higher than those obtained by lower resolution maps. Combining the results from Table I and the mean distance errors in Fig. 18, the best performance of the DeepMap system is achieved when the resolution of an RSS radio map is set to 200 cm. At this resolution, map construction and testing times decrease to 1.24 and 0.11 s, respectively. With the help of this shorter testing time, DeepMap has the potential to provide real-time localization and navigation services to indoor mobile device users. Additionally, at this optimal resolution, map size is only 0.83 MB, which can fit on most mobile devices.

VI. CONCLUSION

In this article, we presented the DeepMap system, a deep Gaussian process model for indoor radio map construction and location estimation. Compared to traditional Gaussian process models for constructing radio maps, the DeepMap system consists of a two-layer deep Gaussian process model that is able to extract nonlinear characteristics from RSS samples. We also proposed a Bayesian training method to optimize the model parameters in the offline stage and a Bayesian fusion algorithm in the online stage for location estimation. We conducted

extensive experiments to evaluate DeepMap's performance using two data sets. The results indicated that DeepMap outperforms the Gaussian process-based baseline scheme in all the experiments with respect to location precision and that it is robust to deficient training data.

REFERENCES

[1] J. Zhang, Y. Lyu, J. Patton, S. C. G. Periaswamy, and T. Roppel, "BFVP: A probabilistic UHF RFID tag localization algorithm using Bayesian filter and a variable power RFID model," *IEEE Trans. Ind. Electron.*, vol. 65, no. 10, pp. 8250–8259, Oct. 2018.

[2] X. Wang, Z. Yu, and S. Mao, "DeepML: Deep LSTM for indoor localization with smartphone magnetic and light sensors," in *Proc. IEEE Int. Conf. Commun. (ICC)*, Kansas City, MO, USA, Jul. 2018, pp. 1–6.

[3] C. Yang, X. Wang, and S. Mao, "SparseTag: High-precision backscatter indoor localization with sparse RFID tag arrays," in *Proc. IEEE Annu. Commun. Soc. Conf. Sensor Mesh Ad Hoc Commun. Netw. (SECON)*, Boston, MA, USA, Jun. 2019, pp. 1–9.

[4] H. Zhu, Y. Zhang, Z. Liu, S. Chang, and Y. Chen, "HyperEar: Indoor remote object finding with a single phone," in *Proc. IEEE Int. Conf. Distrib. Comput. Syst. (ICDCS)*, Dallas, TX, USA, Jul. 2019, pp. 678–687.

[5] L. Yang, Y. Chen, X.-Y. Li, C. Xiao, M. Li, and Y. Liu, "Tagoram: Real-time tracking of mobile RFID tags to high precision using COTS devices," in *Proc. ACM Mobicom*, Sep. 2014, pp. 237–248.

[6] X. Wang, S. Mao, S. Pandey, and P. Agrawal, "CA^{2}T: Cooperative antenna arrays technique for pinpoint indoor localization," in *Proc. MobiSPC*, Aug. 2014, pp. 392–399.

[7] X. Wang, H. Zhou, S. Mao, S. Pandey, P. Agrawal, and D. M. Bevly, "Mobility improves LMI-based cooperative indoor localization," in *Proc. IEEE Wireless Commun. Netw. Conf. (WCNC)*, Mar. 2015, pp. 2215–2220.

[8] J. Zhang *et al.*, "RFHUI: An intuitive and easy-to-operate human-UAV interaction system for controlling a UAV in a 3D space," in *Proc. EAI MobiQuitous*, New York, NY, USA, Nov. 2018, pp. 69–76.

[9] J. Zhang *et al.*, "RFHUI: An RFID based human-unmanned aerial vehicle interaction system in an indoor environment," *Digit. Commun. Netw. J.*, vol. 6, no. 1, pp. 14–22, Feb. 2020.

[10] Y. Xie, J. Xiong, M. Li, and K. Jamieson, "mD-Track: Leveraging multi-dimensionality in passive indoor Wi-Fi tracking," in *Proc. ACM MobiCom*, Oct. 2019, pp. 1–16.

[11] H. Liu, H. Darabi, P. Banerjee, and L. Jing, "Survey of wireless indoor positioning techniques and systems," *IEEE Trans. Syst., Man, Cybern. C, Appl. Rev.*, vol. 37, no. 6, pp. 1067–1080, Nov. 2007.

[12] P. Bahl and V. N. Padmanabhan, "RADAR: An in-building RF-based user location and tracking system," in *Proc. IEEE INFOCOM*, Tel Aviv, Israel, Mar. 2000, pp. 775–784.

[13] M. Youssef and A. K. Agrawala, "The Horus WLAN location determination system," in *Proc. ACM MobiSys*, Seattle, WA, USA, Jun. 2005, pp. 205–218.

[14] X. Wang, L. Gao, S. Mao, and S. Pandey, "CSI-based fingerprinting for indoor localization: A deep learning approach," *IEEE Trans. Veh. Technol.*, vol. 66, no. 1, pp. 763–776, Jan. 2017.

[15] X. Wang, L. Gao, and S. Mao, "CSI phase fingerprinting for indoor localization with a deep learning approach," *IEEE Internet Things J.*, vol. 3, no. 6, pp. 1113–1123, Dec. 2016.

[16] X. Wang, L. Gao, and S. Mao, "BiLoc: Bi-modality deep learning for indoor localization with 5GHz commodity Wi-Fi," *IEEE Access*, vol. 5, pp. 4209–4220, 2017.

[17] X. Wang, X. Wang, and S. Mao, "CiFi: Deep convolutional neural networks for indoor localization with 5GHz Wi-Fi," in *Proc. IEEE Int. Conf. Commun. (ICC)*, Paris, France, May 2017, pp. 1–6.

[18] W. Wang, X. Wang, and S. Mao, "Deep convolutional neural networks for indoor localization with CSI images," *IEEE Trans. Netw. Sci. Eng.*, vol. 7, no. 1, pp. 316–327, Jan.–Mar. 2020, doi: 10.1109/TNSE.2018.2871165.

[19] X. Wang, X. Wang, and S. Mao, "ResLoc: Deep residual sharing learning for indoor localization with CSI tensors," in *Proc. IEEE PIMRC*, Oct. 2017, pp. 1–6.

[20] A. Schwaighofer, M. Grigoras, V. Tresp, and C. Hoffmann, "GPPS: A Gaussian process positioning system for cellular networks," in *Proc. NIPS*, Whistler, BC, Canada, Dec. 2003, pp. 579–586.

[21] S. He and S.-H. G. Chan, "Towards crowdsourced signal map construction via implicit interaction of IoT devices," in *Proc. IEEE SECON*, San Diego, CA, USA, Jun. 2017, pp. 1–9.

[22] F. Duvallet and A. D. Tews, "WiFi position estimation in industrial environments using Gaussian processes," in *Proc. IEEE/RSJ Int. Conf. Intell. Robots Syst.*, Nice, France, Sep. 2008, pp. 2216–2221.

[23] M. Dashti, S. Yiu, S. Yousefi, F. Perez-Cruz, and H. Claussen, "RSSI localization with Gaussian processes and tracking," in *Proc. IEEE Globecom Workshops*, San Diego, CA, USA, Dec. 2015, pp. 1–6.

[24] W. Zhang, H. Huang, and X. Tian, "Gaussian process based radio map construction for LTE localization," in *Proc. IEEE WCSP*, Nanjing, China, Oct. 2017, pp. 1–6.

[25] F. Seco, C. Plagemann, A. R. Jiménez, and W. Burgard, "Improving RFID-based indoor positioning accuracy using Gaussian processes," in *Proc. IEEE IPIN*, Sep. 2010, pp. 1–8.

[26] H. Wymeersch, S. Maranò, W. M. Gifford, and M. Z. Win, "A machine learning approach to ranging error mitigation for UWB localization," *IEEE Trans. Commun.*, vol. 60, no. 6, pp. 1719–1728, Jun. 2012.

[27] C. E. Rasmussen and C. K. I. Williams, *Gaussian Processes for Machine Learning*. Cambridge, MA, USA: MIT Press, 2006.

[28] X. Wang, X. Wang, S. Mao, J. Zhang, S. C. G. Periaswamy, and J. Patton, "DeepMap: Deep Gaussian process for indoor radio map construction and location estimation," in *Proc. IEEE GLOBECOM*, Abu Dhabi, UAE, Dec. 2018, pp. 1–7.

[29] A. Damianou and N. Lawrence, "Deep Gaussian processes," in *Proc. 16th Int. Conf. Artificial Intell. Stat.*, Scottsdale, AZ, USA, May 2013, pp. 207–215.

[30] J. Xiao, K. Wu, Y. Yi, and L. M. Ni, "FIFS: Fine-grained indoor fingerprinting system," in *Proc. IEEE ICCCN*, Munich, Germany, Aug. 2012, pp. 1–7.

[31] S. Sen, B. Radunovic, R. R. Choudhury, and T. Minka, "You are facing the Mona Lisa: Spot localization using PHY layer information," in *Proc. ACM MobiSys*, Low Wood Bay, U.K., Jun. 2012, pp. 183–196.

[32] X. Wang, L. Gao, S. Mao, and S. Pandey, "DeepFi: Deep learning for indoor fingerprinting using channel state information," in *Proc. WCNC*, New Orleans, LA, USA, Mar. 2015, pp. 1666–1671.

[33] X. Wang, L. Gao, and S. Mao, "PhaseFi: Phase fingerprinting for indoor localization with a deep learning approach," in *Proc. GLOBECOM*, San Diego, CA, USA, Dec. 2015, pp. 1–6.

[34] J. Wang, X. Zhang, Q. Gao, H. Yue, and H. Wang, "Device-free wireless localization and activity recognition: A deep learning approach," *IEEE Trans. Veh. Technol.*, vol. 66, no. 7, pp. 6258–6267, Jul. 2017.

[35] M. Abbas, M. Elhamsharyand, H. Rizk, M. Torki, and M. Youssef, "WiDeep: WiFi-based accurate and robust indoor localization system using deep learning," in *Proc. IEEE PerCom*, Kyoto, Japan, Mar. 2019, pp. 1–10.

[36] X. Chen, C. Ma, M. Allegue, and X. Liu, "Taming the inconsistency of Wi-Fi fingerprints for device-free passive indoor localization," in *Proc. IEEE INFOCOM*, Atlanta, GA, USA, May 2017, pp. 1–9.

[37] W. Shao, H. Luo, F. Zhao, Y. Ma, Z. Zhao, and A. Crivello, "Indoor positioning based on fingerprint-image and deep learning," *IEEE Access*, vol. 6, pp. 74699–74712, 2018.

[38] S. Kumar, R. M. Hegde, and N. Trigoni, "Gaussian process regression for fingerprinting based localization," *Ad Hoc Netw.*, vol. 51, pp. 1–10, Nov. 2016.

[39] H. Zou, M. Jin, H. Jiang, L. Xie, and C. Spanos, "WinIPS: WiFi-based non-intrusive indoor positioning system with online radio map construction and adaptation," *IEEE Trans. Wireless Commun.*, vol. 16, no. 12, pp. 8118–8130, Dec. 2017.

[40] Y. Tao and L. Zhao, "A novel system for WiFi radio map automatic adaptation and indoor positioning," *IEEE Trans. Veh. Technol.*, vol. 67, no. 11, pp. 10683–10692, Nov. 2018.

[41] M. K. Titsias and N. D. Lawrence, "Bayesian Gaussian process latent variable model," in *Proc. 13th Int. Conf. Artif. Intell. Stat.*, Sardinia, Italy, May 2010, pp. 844–851.

[42] S. Kullback, *Information Theory and Statistics*. Hoboken, NJ, USA: Wiley, 1959.

[43] G. Jekabsons and V. Zuravlyov, "Refining Wi-Fi based indoor positioning," in *Proc. 4th Int. Sci. Conf. Appl. Inf. Commun. Technol. (AICT)*, Jelgava, Latvia, Oct. 2010, pp. 87–95.